

Zero-energy states in graphene quantum dot with wedge disclination

Ahmed Bouhlal,¹ Ahmed Jellal,^{1,2} and Nurisya Mohd Shah^{3,4}

¹*Laboratory of Theoretical Physics, Faculty of Sciences,
Chouaib Doukkali University, PO Box 20, 24000 El Jadida, Morocco*

²*Canadian Quantum Research Center, 204-3002 32 Ave Vernon, BC V1T 2L7, Canada*

³*Laboratory of Computational Sciences and Mathematical Physics, Institute for Mathematical Research (INSPEM),
Universiti Putra Malaysia, 43400 UPM Serdang, Selangor, Malaysia*

⁴*Department of Physics, Faculty of Science, Universiti Putra Malaysia, 43400 UPM Serdang, Selangor, Malaysia*

We investigate the effects of wedge disclination on charge carriers in circular graphene quantum dots subjected to a magnetic flux. Using the asymptotic solutions of the energy spectrum for large arguments, we approximate the scattering matrix elements, and then study the density of states. It is found that the density of states shows several resonance peaks under various conditions. In particular, it is shown that the wedge disclination is able to change the amplitude, width, and positions of resonance peaks.

PACS numbers: 81.05.ue; 73.63.-b; 73.23.-b; 73.22.Pr

KEYWORDS: Graphene, quantum dot, electrostatic potential, magnetic flux, wedge disclination, density of states.

I. INTRODUCTION

Graphene is the focus of much theoretical and experimental research due to its electronic and optical properties [1–4]. Graphene has become a primary material for future nanoelectronic devices [5]. Most of the research conducted so far is based on the mobility of electrons, which is determined by the diffusion of charged impurities [6, 7]. The two graphene conduction and valence bands touch each other at two asymmetric points noted (K, K') are called Dirac points. In the vicinity of these Dirac points, the energy dispersion is linear, which is the origin of graphene's unique electronic properties like high electrical conductivity [5, 8]. At normal incidence, the electrons transmit completely, which is due to a Klein tunneling effect, and it is therefore difficult to control them with external fields in the graphene [9–11]. However, it has been shown theoretically that it is still possible to create quasi-bound states (QBS) using external electric fields such as the magnetic field [12–14].

The notion of quantum dots is used in modern physics to study some physical phenomena. It is essential to the progress of quantum computing and spintronics. The reasons for choosing the application of graphene are twofold: on the one hand, because graphene is considered a two-dimensional zero energy gap system [15] and on the other hand, because the quantum dots in graphene have the potential to be used as spin qubits [16]. The study of the possibility of electron confinement in graphene quantum dots is particularly important in this context [17, 18]. The experimental activity will be based on the confinement of Dirac fermions in graphene quantum dots [19]. Due to the absence of a band gap, the confinement of charge carriers under the effect of an electrostatic potential using metallic gates is impossible in graphene. The use of a magnetic flux in graphene quantum dots allows for better control and confinement of fermions in the presence of an electrostatic potential [20]. It is well

demonstrated that the magnetic flux is responsible for the kinematic angular momentum taking integer values, allowing the appearance of states that cannot be confined by the electrostatic potential alone [21]. The disk-shaped quantum dot has a circular symmetry from which the angle of incidence is a characteristic of the movement of electrons, knowing that the latter at their non-zero angular momentum are confined within the quantum dot [14, 22]. Like graphene, it is well demonstrated that it is an ideal two-dimensional system where the energy dispersion is linear and has a density of states that cancels at zero energy [5]. In this work, we study electrostatic confinement in the presence of magnetic flux with wedge disclination.

Insulators and superconductors react significantly to topological defects and exhibit quasi-zero energy states around the defect [23]. The effect of a Coulombian electrostatic potential in the presence of a uniform magnetic field on the energy spectrum of graphene has been studied recently [24]. Prior to the year 2014, two-terminal conductance was the only technique used to study the confinement of Dirac fermions in a graphene quantum dot [14, 25, 26]. In 2014, Martin Schneider developed a technique based on density of states (DOS) analysis to study the possibility of confinement in a small graphene region [27]. These studies are extended by examining how the information of the confinement signature has been deduced by the analysis of the density of states, and in parallel, the effect of the gap energy on the information of the system has also been studied [28]. We wish to consider in this context the simple disclination via the construction of Volterra [29]. Our goal in this paper is to investigate the properties of a graphene monolayer in which the crystal symmetry is locally modified by the conical geometry mentioned above.

We consider a circular graphene quantum dot of radius R surrounded by a circular ring of undoped graphene of external radius L bound by a metallic contact in the

presence of a magnetic field with a wedge disclination $n = 0, \pm 1, \pm 2$. By restricting ourselves to the asymptotic behavior of Hankel functions for large arguments, we determine the scattering matrix. DOS is calculated as a function of magnetic flux Φ , applied electrostatic potential V_0 , and wedge disclination n . We numerically analyze the DOS under various conditions of the physical parameters. This allows us to show different oscillatory behaviors and to find resonances. We show that the DOS peaks strongly depend on the momentum quantum number m . During the scanning of the gate voltage, the zero energy bound states cause resonant peaks that become narrow if the size L of the undoped graphene sheet containing the quantum dot increases, see Fig. 1. Subsequently, we discover that n acts by changing the resonance peaks. Indeed, this behavior contrasts strongly with that of $n = 2$ (square defect), which moves to the right from its initial position where $n = 0$ (defect-free), and then the resonance becomes more and more acute. In the opposite case, where $n = -2$ (octagon defect), we observe the creation of a new peak that corresponds to $m = 5/2$.

The paper is organized as follows. In section II, we establish a theoretical model describing electrostatically confined charge carriers in geometry obtained by Volterra construction. We calculate the scattering matrix by restricting to the asymptotic behavior of Hankel functions in section III, which are obtained in the solution of the energy spectrum. Using the scattering matrix, we explicitly determine the associated DOS in section IV. In section V, we numerically analyze the DOS and show it exhibits a set of resonance peaks. Under various conditions, the effects of magnetic flux and the wedge n on these peaks will be investigated. Finally, we conclude our results.

II. THEORETICAL MODEL

The configuration we study consists of a graphene quantum dot (QD) connected to a ring-shaped metal contact, and the two are separated by an undoped intrinsic graphene layer. The Hamiltonian of a graphene monolayer that describes the motion of a single electron in the presence of an axially symmetric external potential $V(r)$ at low energy is

$$H = v_F (\tau_z \sigma_x p_x + \sigma_y p_y) + V(r) \quad (1)$$

where $p = (p_x, p_y)$ is the momentum operator, $v_F = 10^6$ m/s is the Fermi velocity, σ_i, τ_i ($i = x, y, z$) are Pauli matrices denoting the sublattice and valley degrees of freedom in the basis of the two sublattices of A and B atoms, respectively. The potential barrier $V(r)$ is defined as follows

$$V(r) = \begin{cases} 0, & R < r < L \\ -\hbar v_F V_0, & r < R \\ -\hbar v_F V_\infty, & r > L \end{cases} \quad (2)$$

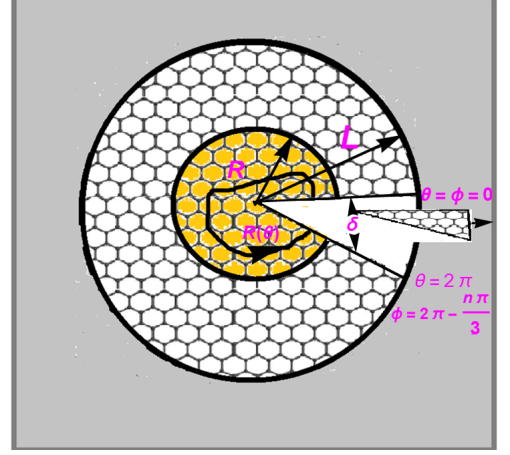


FIG. 1. (color online) Graphene quantum dots of radius R surrounded by an undoped intrinsic graphene sheet in the form of a ring of outer radius L and coupled to source and drain reservoirs with a corner of angle θ removed. $R(\theta)$ is the curve along which the spinor is rotated.

with the parameters V_0 and V_∞ are chosen to be positive because the two regions outside the ring of radius R and L are doped with electrons. The highly doped lead graphene is modeled by taking the limit $V_\infty \rightarrow \infty$. The Hamiltonian (1) acts on the spinor with four components

$$\Psi(\vec{r}) = (\psi_{A+}(\vec{r})\psi_{B+}(\vec{r})\psi_{A-}(\vec{r})\psi_{B-}(\vec{r}))^T \quad (3)$$

where the valley indices $+$ ($-$) refer to the two Dirac points K (K') in the Brillouin zone. For a two dimensional graphene, the angular boundary condition for a Dirac spinor when it follows a closed path is given by

$$\Psi(r, \theta = 2\pi) = e^{i\pi\tau_z\sigma_z} \Psi(r, \theta = 0) \quad (4)$$

and we will see that the presence of the wedge disclination modifies the angular boundary conditions in (4). Indeed, it is known that the deformation in a honeycomb lattice falls in the description at the continuum boundary undergoes a pseudo-gauge field coupled to the electron pulse by a vector potential [30–32]. As shown in Fig. 1, the Volterra construction can be used to introduce the wedge disclination by removing a sector of $\delta = n\pi/3$. The integer n represents the type of disclination in the honeycomb lattice, with $n = -2$ representing an isolated octagon defect, $n = -1$ representing an isolated heptagon defect, $n = 0$ representing an isolated defect in the no defect case, $n = 1$ representing an isolated pentagon defect, and $n = 2$ representing an isolated square defect. As a result, the wave function (4) becomes

$$\Psi(r, \theta = 2\pi) = -e^{i2\pi[1-(n/6)]\tau_z\sigma_z/2} \Psi(r, \theta = 0). \quad (5)$$

Exchanging the K and K' blocks in the Hamiltonian using the unitary transformation $e^{i\pi\sigma_y\tau_y/2}$ yields the angular boundary condition for any number n [33, 34]

$$\Psi(r, \theta = 2\pi) = -e^{i2\pi[-\frac{n}{4}\sigma_y\tau_y + (1-(n/6))\frac{1}{2}\tau_z\sigma_z]} \Psi(r, \theta = 0) \quad (6)$$

For a local gauge transformation, (6) can be written in two singular gauge transformations

$$\Psi(r, \theta = 2\pi) = F(\phi)G_n(\theta)\Psi(r, \theta = 0) \quad (7)$$

where $F(\phi) = e^{i\frac{\phi}{2}\tau_z\sigma_z}$ and $G_n(\theta) = e^{i\frac{n\theta}{4}\tau_y\sigma_y}$, as shown in Fig. 1 with $\theta = \frac{\phi}{1-\frac{n}{6}} \in [0, 2\pi]$.

Let us now consider an external magnetic flux Φ applied to the quantum dot (QD)

$$\vec{A} = \frac{\hbar\Phi}{\Omega_n e\Phi_0 r} \vec{e}_\theta \quad (8)$$

where $\Phi_0 = h/e$ is the flux quantum and \vec{e}_θ is the unit vector along the azimuthal direction and the wedge disclination is described by $\Omega_n = 1 - \frac{n}{6}$ [35] with $n = 0, \pm 1, \pm 2$. For this, we replace the momentum \vec{p} by the conical momentum $\vec{p} + e\vec{A}$ in the Hamiltonian (1) and use the transformations of $F(\phi)$ and $G_n(\theta)$. This process yields

$$\tilde{H}(r, \theta) = F^\dagger G_n^\dagger H G_n F \quad (9)$$

such that the Hamiltonian (1) is now given by

$$\begin{aligned} \tilde{H}(r, \theta) = & \hbar v_F \left(k_r - \frac{i}{2r} \right) \sigma_x \\ & + \hbar v_F \left(k_\theta + \frac{\Phi_i}{\Omega_n r} + \frac{n}{4\Omega_n r} \tau_z \right) \sigma_y + V(r) \end{aligned} \quad (10)$$

where $k_r = -i\frac{\partial}{\partial r}$, $k_\theta = -\frac{i}{r\Omega_n}\frac{\partial}{\partial \theta}$ and $\Phi_i = \frac{\Phi}{\Phi_0}$ is the dimensionless flux. It is easy to verify that the total angular momentum $J_z = L_z + \frac{\hbar}{2}\sigma_z$ commutes with the Hamiltonian (1). As a result, the eigenfunctions can be separated as

$$\Psi(r, \theta) = e^{im\theta} \begin{pmatrix} \chi_A(r) \\ \chi_B(r) \end{pmatrix} \quad (11)$$

with $m = \pm 1/2, \pm 3/2, \dots$ are eigenvalues of J_z .

We solve the eigenvalue equation $H\Psi_\tau = E\Psi_\tau$ in the three regions: $0 < r < R$, $R < r < L$ and $r > L$. After some algebras, we obtain two coupled radial equations

$$\left[\frac{\partial}{\partial r} + \frac{1}{2r} + \frac{1}{r\Omega_n} \left(m + \Phi_i + \frac{n\tau}{4} \right) \right] \chi_B = (\epsilon - V_i) \chi_A \quad (12)$$

$$\left[-\frac{\partial}{\partial r} - \frac{1}{2r} + \frac{1}{r\Omega_n} \left(m + \Phi_i + \frac{n\tau}{4} \right) \right] \chi_A = (\epsilon - V_i) \chi_B \quad (13)$$

where dimensionless parameters $\epsilon = \frac{E}{\hbar v_F}$ and $V_i = \frac{V(r)}{\hbar v_F}$ have been defined. We look for a second order equation for one component and reusing one of (12-13) to find the other component of the wave function. Now, injecting (12) into (13) to end up with

$$\left[\rho^2 \frac{\partial^2}{\partial \rho^2} + \rho \frac{\partial}{\partial \rho} + \rho^2 - \left(\mu - \frac{1}{2} \right)^2 \right] \chi_A(\rho) = 0 \quad (14)$$

where we have set $\mu = \frac{1}{\Omega_n} \left(m + \Phi_i + \frac{n\tau}{4} \right)$ and $\rho = kr$ with $k = \epsilon - V_i$ is the wave number. (14) can be reformulated as the Bessel differential equation. In general, the solution is a linear combination of the Hankel function of first $H_n^+(\rho)$ and of second $H_n^-(\rho)$ kinds. Then we combine them to get the proper eigenspinors

$$\psi_{k,\mu}^\pm(r) = e^{i(\mu-\frac{1}{2})\theta} \sqrt{\frac{k}{4\pi}} \begin{pmatrix} H_{\mu-1/2}^\pm(kr) \\ i \text{sign}(\mu) e^{i\theta} H_{\mu+1/2}^\pm(kr) \end{pmatrix} \quad (15)$$

which describe incoming (-) (propagating from $r = 0$) or outgoing (+) (propagating from $r = \infty$) for circular waves. Note that, $H_n^{(\pm)}$ are linear combinations of Bessel J_n and Neumann Y_n , namely $H_n^{(\pm)} = J_n \pm iY_n$. We specify the value of k which differs from one region to another where the solutions (15) apply. For $r < R$: $k \equiv k_0 = \epsilon + V_0$, for $R < r < L$: $k = \epsilon$ and for $r > L$: $k \equiv k_\infty = \epsilon + V_\infty$. Recall that the half-integer Bessel functions are valid, i.e., $Y_{1/2}(x) = -J_{1/2}(x) = -\sqrt{\frac{2}{\pi x}} \cos x$, $Y_{-1/2}(x) = J_{1/2}(x) = \sqrt{\frac{2}{\pi x}} \sin x$. It is clearly seen that the function $\frac{\cos(kr)}{\sqrt{r}}$ is divergent at the origin. Therefore for $\mu = 0$, we have

$$\psi_{\kappa,0}^\pm(r) = \frac{e^{\pm i\kappa r}}{\sqrt{8\pi^2 r}} \begin{pmatrix} \pm e^{-i\theta} \\ 1 \end{pmatrix}. \quad (16)$$

At the center of the quantum dot ($R \rightarrow 0$) and for the wave function to be regular at $r = 0$, we have the solution inside the quantum dot ($r < R$)

$$\psi_{k,\mu}(r) = e^{i(\mu-\frac{1}{2})\theta} \sqrt{\frac{k_0}{4\pi}} \begin{pmatrix} J_{\mu-1/2}(kr) \\ i \text{sign}(\mu) e^{i\theta} J_{\mu+1/2}(kr) \end{pmatrix} \quad (17)$$

For the region $R < r < L$, the eigenspinors can be written as a linear combination of the two solutions of (15)

$$\psi_2(r) = a_\mu \psi_{k,\mu}^-(r) + b_\mu \psi_{k,\mu}^+(r) \quad (18)$$

with a_μ, b_μ being arbitrary constants. Inside the circular ring $R < r < L$ and at zero energy ($\epsilon = 0$), the radial components have the forms

$$\chi_A(r) = a_+ r^{\mu-\frac{1}{2}}, \quad \chi_B(r) = a_- r^{-\mu-\frac{1}{2}}. \quad (19)$$

To avoid divergence, we require the constraints $a_+ = 0$ for $\mu > 0$ and $a_- = 0$ for $\mu < 0$.

We use the asymptotic behavior of Hankel functions in the limit of a heavily doped lead where $k_\infty L \gg 1$. That is

$$H_n^{(\pm)}(x) \approx (2/\pi x)^{1/2} e^{\pm i(x - n\frac{\pi}{2} - \frac{\pi}{4})}. \quad (20)$$

As a result the eigenspinors $\psi_1(r)$ inside the quantum dot ($r < R$) and $\psi_3(r)$ outside the quantum ring ($r > L$) can be simplified to

$$\psi_1(r) = \sqrt{k_0} \begin{pmatrix} J_{\mu-1/2}(k_0 r) \\ J_{\mu+1/2}(k_0 r) \end{pmatrix} \quad (21)$$

$$\psi_3(r) = c_\mu \frac{e^{-ik_\infty r}}{\sqrt{r}} \begin{pmatrix} 1 \\ -1 \end{pmatrix} + d_\mu \frac{e^{ik_\infty r}}{\sqrt{r}} \begin{pmatrix} 1 \\ 1 \end{pmatrix} \quad (22)$$

III. SCATTERING MATRIX

The coefficients $a_\mu(\epsilon)$, $b_\mu(\epsilon)$, $c_\mu(\epsilon)$ and $d_\mu(\epsilon)$ can be determined using the continuity of the wave function at $r = R$ and $r = L$ and the regularity at $r = 0$. The first

$$D^{(\pm)} = \begin{pmatrix} 0 & \sqrt{k}H_{\mu-\frac{1}{2}}^{(+)}(kR) & \sqrt{k}H_{\mu-\frac{1}{2}}^{(-)}(kR) & \sqrt{k_0}J_{\mu-\frac{1}{2}}(k_0R) \\ 0 & \sqrt{k}H_{\mu+\frac{1}{2}}^{(+)}(kR) & \sqrt{k}H_{\mu+\frac{1}{2}}^{(-)}(kR) & \sqrt{k_0}J_{\mu+\frac{1}{2}}(k_0R) \\ \frac{e^{\mp ik_\infty L}}{\sqrt{L}} & -\sqrt{k}H_{\mu-\frac{1}{2}}^{(+)}(kL) & -\sqrt{k}H_{\mu-\frac{1}{2}}^{(-)}(kL) & 0 \\ \frac{e^{\mp ik_\infty L}}{\sqrt{L}} & -i\sqrt{k}H_{\mu+\frac{1}{2}}^{(+)}(kL) & -i\sqrt{k}H_{\mu+\frac{1}{2}}^{(-)}(kL) & 0 \end{pmatrix}. \quad (25)$$

For small distances, we have

$$J_n(x) \sim \frac{1}{n!} \left(\frac{x}{2}\right)^n \quad (26)$$

$$Y_n(x) \sim \begin{cases} -\frac{\Gamma(n)}{\pi} \left(\frac{x}{2}\right)^n, & n > 0 \\ \frac{2}{\pi} \ln\left(\gamma_E \frac{x}{2}\right), & n = 0 \end{cases} \quad (27)$$

with $\ln(\gamma_E) = 0.577 \dots$ is defined as an Euler constant. Indeed, for small ϵ , we can develop the scattering matrix as a function of k in the internal region ($R < r < L$). Then, we write

$$S_\mu(\epsilon) = e^{-2ik_\infty L + i|\mu|\pi} \left[S_\mu^{(0)} + kL S_\mu^{(1)} + \mathcal{O}(\epsilon^2) \right] \quad (28)$$

such that

$$S_\mu^{(0)} = \frac{1 + i\mathcal{J}_\mu R_L^{2|\mu|}}{1 - i\mathcal{J}_\mu R_L^{2|\mu|}} \quad (29)$$

and we used the abbreviation

$$\mathcal{J}_\mu = \frac{J_{|\mu|+\frac{1}{2}}(k_0R)}{J_{|\mu|-\frac{1}{2}}(k_0R)} \quad (30)$$

where $R_L = \frac{R}{L}$. We distinguish two cases for $S_\mu^{(1)}$. Indeed, in the absence of magnetic flux and in the defect-free case ($\phi = 0, n = 0$), we have

$$S_\mu^{(1)} = -\frac{2i}{2|\mu|-1} S_\mu^{(0)} + \frac{8i|\mu| + 2i[(2|\mu|+1)\mathcal{J}_\mu^2 - (2|j|-1)]R_L^{2|\mu|+1}}{(4|\mu|^2-1)(1-i\mathcal{J}_j R_L^{2|\mu|})^2} \quad (31)$$

as well as for $|\mu| = \frac{1}{2}$

$$S_{\pm 1/2}^{(1)} = \frac{i(1-R_L^2) - 2i\mathcal{J}_{\frac{1}{2}}^2 R_L^2 \ln(R_L)}{(1-i\mathcal{J}_{\frac{1}{2}} R_L)^2}. \quad (32)$$

In the presence of magnetic flux and wedge disclination, we find that the results of (31) remain valid for $\mu \neq 0$. We

two coefficients are linked via the scattering matrix $S_\mu(\epsilon)$

$$d_\mu(\epsilon) = S_\mu(\epsilon)c_\mu(\epsilon) \quad (23)$$

$$S_\mu(\epsilon) = -\frac{\det D^{(-)}}{\det D^{(+)}} \quad (24)$$

where the matrices $D^{(\pm)}$ are given by

compute the scattering matrix $S_0(\epsilon)$ for the case $\mu = 0$. We show that it is constant and independent of V_0 , such as

$$S_0 = e^{-2i(k_\infty - k_0)R} e^{-2i(k - k_\infty)(R-L)}. \quad (33)$$

IV. DENSITY OF STATES

Using the scattering matrix for low energy (28), we will calculate the density of states at zero energy in terms of the potential $V(r)$. The local density of states (LDOS) $\rho(r, \epsilon)$ is given by the derivative of the scattering matrix $S(\epsilon, V(r))$ [36–38]

$$\rho(r, \epsilon) = -\frac{1}{2\pi i} \text{Tr} S_\mu(\epsilon, V(r))^\dagger \left(\frac{\delta S_\mu(\epsilon, V(r))}{\delta V(r)} \right). \quad (34)$$

We calculate the total density of states (DOS) of the circular quantum dot by integrating $\rho(r, \epsilon)$ in region $r < L$ [27]. This yields to

$$\rho_{dot}(\epsilon) = -\frac{1}{2\pi i} \int_{r < L} \text{Tr} S_\mu(\epsilon, V(r))^\dagger \left(\frac{\delta S_\mu(\epsilon, V(r))}{\delta V(r)} \right) dr. \quad (35)$$

We can now calculate ρ_{dot} at zero energy using (35), which gives

$$\rho_{dot} = \frac{1}{2\pi i \hbar v_F} \sum_\mu S_\mu^{(0)*} \left[\frac{\partial S_\mu^{(0)}}{\partial V_0} + L S_\mu^{(1)} \right]. \quad (36)$$

It is worth noting that DOS is related to the point conductance [27, 39] and is dependent on the Wigner-Smith delay [40].

Taking into account the continuity of the eigenspinors (17) and (19) at $r = R$ for zero energy, the resonance condition is well established

$$J_{|\mu|-1/2}(V_0' R) = 0 \quad (37)$$

value and $\tau = 1$, we observe that the resonance peaks change their initial positions and move to the left, which explains the appearance of three peaks corresponding to $m = 5/2$, $m = 11/2$ and $m = 13/2$ when $n = -2$ and $\tau = 1$. Their amplitudes decrease as the size of the width increases. In the opposite case where $\tau = -1$, the effect of wedge disclination n is reversed, such that for negative values of n with $\tau = -1$, the resonance peaks move to the right with an increase in amplitude and a decrease in width. The condition (37) shows that there are three resonance peaks that are labeled according to their angular momentum $m = 1/2$. However, they are missing for two cases: $(n = 2, \tau = -1)$ and $(n = -2, \tau = 1)$, as shown in Fig. 2f,i.

The characteristics of the resonance are found to be dependent on the value of n and the valley τ . The resonance positions shift to the right if $\tau n > 0$ and become very straight and very important for $n = 2$ and $\tau = 1$, whereas they shift to the left for $\tau n < 0$. When $n > 0$, the influence of this magnitude where $n > 0$ on the behavior of the resonance peaks is reversed. This result becomes very clear when the DOS is plotted in Fig. 3 for the first or the second resonance by varying the values of n and τ . In the case where $\tau = -1$, the parameter n has no effect on the position or characteristics of the second resonance peak, as shown in Fig. 3d. We note that the peaks of the second DOS resonance are very narrow compared to those of the first resonance. As n increases in Fig. 3c, the resonance peaks become very narrow, such that their amplitude increases but their width decreases.

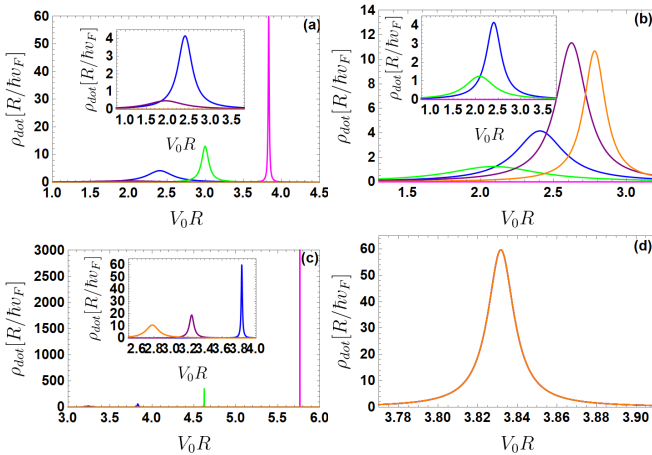


FIG. 3. (color online) DOS as a function of gate voltage $V_0 R$ at $\epsilon = 0$ with $R/L = 0.2$, $\Phi_i = 0$ for $n = 0$ (blue line), $n = 1$ (green line), $n = 2$ (magenta line), $n = -1$ (purple line), $n = -2$ (orange line). (a, b): $m = 1/2$ and (c, d): $m = 3/2$ with (a, c): $\tau = 1$ and (b, d): $\tau = -1$.

In Fig. 4, we only consider the first resonance and investigate its influence on the magnitude of the point-lead coupling R/L , where L denotes the distance between the source and the drain. We observe that the resonance peaks have Lorentzian shapes whose properties depend

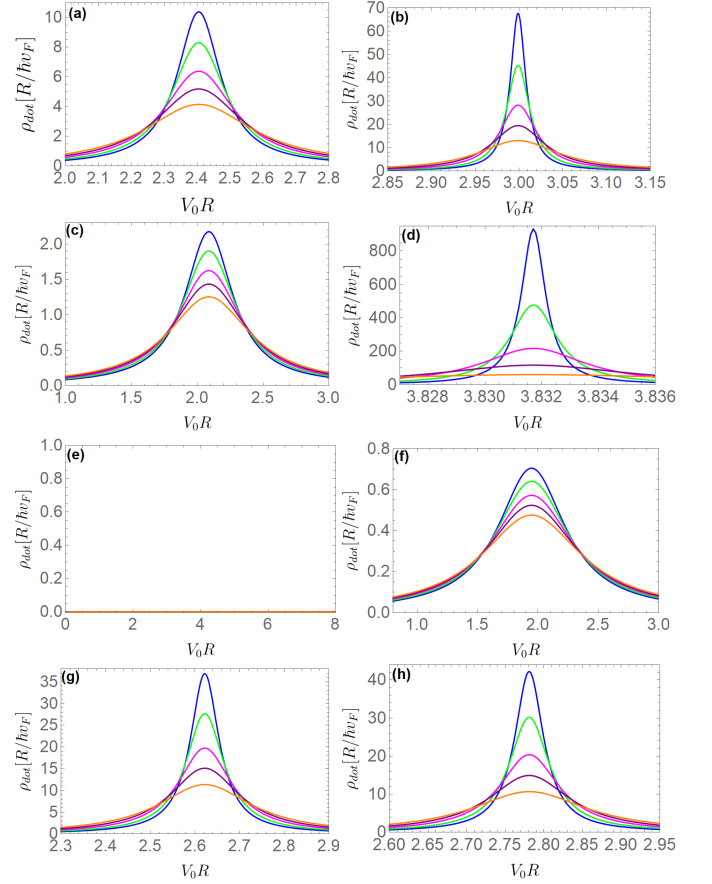


FIG. 4. (color online) DOS as a function of gate voltage $V_0 R$ at $\epsilon = 0$ with $\Phi_i = 0$ for $m = 1/2$ by changing the ratio $R/L = 0.08$ (blue line), $R/L = 0.1$ (green line), $R/L = 0.13$ (magenta line), $R/L = 0.16$ (purple line), $R/L = 0.2$ (orange line). The pair (n, τ) is (a): 0, (b): (1, 1), (c): (1, -1), (d): (2, 1), (e): $(\pm 2, \mp 1)$, (f): $(-1, 1)$, (g): $(-1, -1)$, (h): $(-2, -1)$.

on several parameters, including the index n and the ratio R/L . The resonance peaks become narrower when the quantum dot is very far from the source, i.e., when $R/L = 0$, as well as when the defect is chosen to be of square type, $n = 2$, and for the valley K ($\tau = 1$). As a result, the DOS is a series of peaks influenced by the gate voltage $V_0 R$, n , R/L , m , and τ . The width of the resonances is independent of the coupling to the source and drain, which is determined by R/L , and the height increases when R/L is very low, $n = 2$, and $\tau = 1$.

The width of the resonance peak as a function of wedge disclination n is shown in Fig. 5 for $m = 1/2, 3/2, 5/2, 7/2$, and $\tau = \pm 1$. For higher values of m with $n = 2$ and $\tau = 1$, one sees that the resonances become very sharp, which is consistent with the width scale (37). The results presented in both Fig. 5b and Fig. 3d show that there is no influence of n on the characteristics and position of the second resonance peak for $\tau = -1$. On the other hand, the variation of the amplitude of resonance peaks is inversely related to the variation of their width. Consequently, these numerical values confirm the

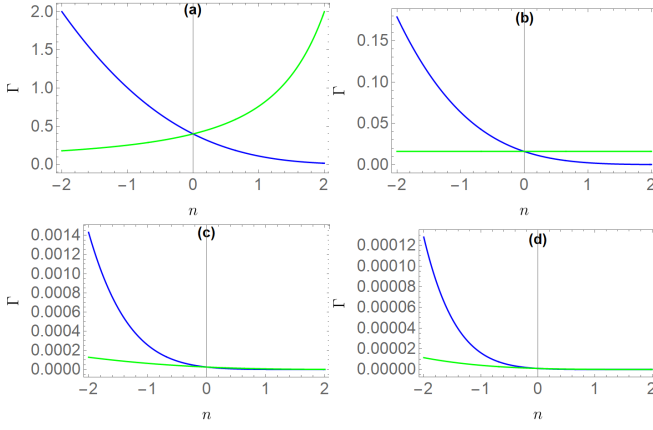


FIG. 5. (color online) The width of resonance peak as a function of wedge disclination n at $\epsilon = 0$ with $R/L = 0.2$, $\Phi_i = 0$ for (a): $m = 1/2$, (b): $m = 3/2$, (c): $m = 5/2$, and (d): $m = 7/2$, $\tau = 1$ (blue line) and $\tau = -1$ (green line).

results obtained above.

We now introduce a magnetic flux carried by a half magnetic flux of $\Phi_i = 1/2$, yielding an integer total angular momentum denoted by μ , which labels the resonance peaks. In Fig. 6, the DOS is shown as a function of the gate voltage $V_0 R$, with $R/L = 0.2$ for $n = 0, \pm 1, \pm 2$, and $\tau = \pm 1$. The electrons circling the flux tube collect an Aharonov-Bohm phase π , canceling out the effect of the Berry phase, and the electron wave function collects via pseudo-rotation while moving in a circular motion. We find that when $\Phi_i = 1/2$, the system enters a state with zero angular momentum, $\mu = 0$, which cannot be confined by an electrostatic potential, even in the presence of a magnetic field. We obtain results that are consistent with previous simulations [14, 27, 28, 41] in terms of the position and scale of the width by changing the resonances R/L when $n = 0$ in Fig. 6. Furthermore, one can observe extremely small resonance peaks in the presence of a magnetic flux.

For $\tau = \pm 1$, the DOS of the first and second resonances $\mu = 1, 2$ is represented in Fig. 7 by varying the value of the wedge disclination $n = 0$ (blue line), $n = 1$ (green line), $n = 2$ (magenta line), $n = -1$ (purple line), and $n = -2$ (orange line).

We notice that the effect of a wedge disclination becomes very important, as shown in Fig. 6e for $n = 2$ and $\tau = 1$. We find very narrow resonance peaks well shifted to the right, which leads to a suppression of the four peaks. For $(n = -2, \tau = 1)$ and under the influence of a magnetic flux, however, we notice a decrease in the amplitude of the peaks as well as the appearance of three peaks, indicating that the number of bound states increases, see Fig. 6.

We investigate the effect of the ratio R/L on DOS for the first resonance $\mu = 1$ in the presence of a magnetic flux $\Phi_i = 1/2$ with $\tau = \pm 1$ by varying the value of a wedge disclination n . By comparing the results of the two Figs. 4 and 9, we show that the analysis can be

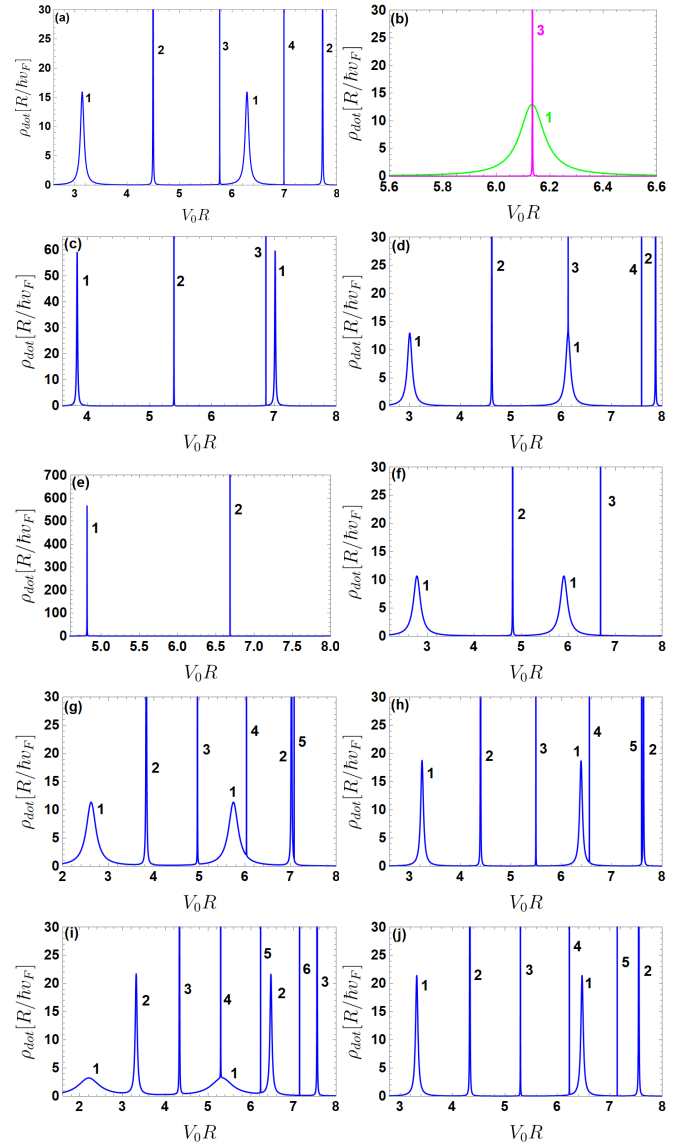


FIG. 6. (color online) DOS as a function of gate voltage $V_0 R$ at $\epsilon = 0$ with $R/L = 0.2$, $\Phi_i = \frac{1}{2}$ for (n, τ) such that (a): 0, (c): (1, 1), (d): (1, -1), (e): (2, 1), (f): (2, -1), (g): (-1, 1), (h): (-1, -1), (i): (-2, 1), (j): (-2, -1). Here (b) is a zoom of (d) for $5.6 < V_0 R < 6.6$ and resonances are labeled by $|\mu| = 1, \dots, 6$.

made quantitative by taking a specific peak and studying the effect of the ratio R/L . We observe that DOS becomes very saturated when the limit $R/L \rightarrow 0$, which corresponds to a weak coupling between the quantum dot and a ring-shaped metallic. Finally, the behavior of the resonance peaks is affected by three physical quantities, which are the wedge disclination value n , the magnetic flux $\Phi_i = 1/2$, and the ratio R/L . To give a better representation of the result, we draw another curve that represents the width of the resonance peaks in the presence of magnetic flux $\Phi_i = 1/2$.

The width of the resonance peak for $\mu = 1, 2, 3, 4$ is

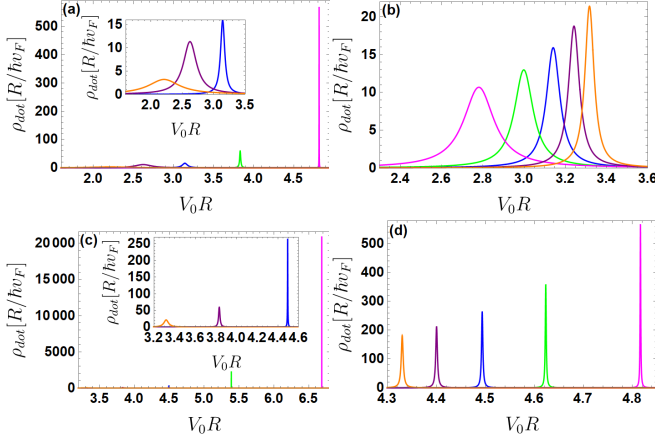


FIG. 7. (color online) DOS as a function of gate voltage $V_0 R$ at $\epsilon = 0$ with $R/L = 0.2$, $\Phi_i = 1/2$ for various wedge of disclination values: $n = 0$ (blue line), $n = 1$ (green line), $n = 2$ (magenta line), $n = -1$ (purple line), $n = -2$ (orange line). (a, b): $\mu = 1$ and (c, d): $\mu = 2$ with (a, c): $\tau = 1$ and (b, d): $\tau = -1$.

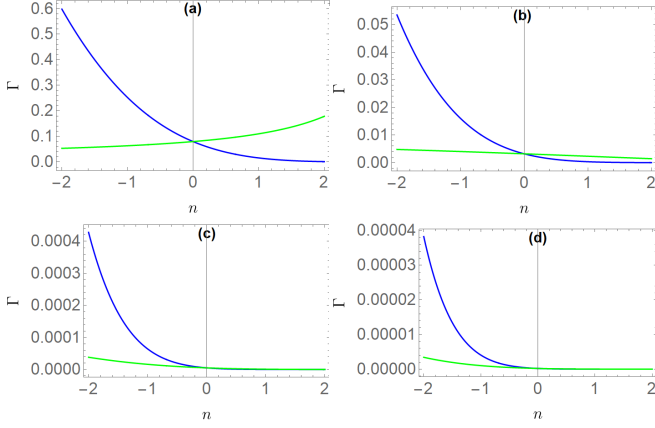


FIG. 8. (color online) The width of the resonance peak as a function of wedge disclination n at $\epsilon = 0$ with $R/L = 0.2$, $\Phi_i = \frac{1}{2}$ for (a): $\mu = 1$, (b): $\mu = 2$, (c): $\mu = 3$ and (d): $\mu = 4$ such that $\tau = 1$ (blue line) and $\tau = -1$ (green line).

plotted in Fig. 8 for two values of $\tau = +1(-1)$. Comparing the results of the two Fig. 5 and Fig. 8, we see that the wedge disclination effect becomes very important for the valley $K(\tau = 1)$. Also, we notice that its effect enjoys the presence of a magnetic flux and for $\tau = 1$, because it is better.

The amplitude of a DOS resonance peak as a function of magnetic flux Φ_i for the angular momentum $m = 1/2$ and wedge disclination $n = 1, 2$ is shown in Fig. 10. We see that the amplitude of a resonance peak grows exponentially as a function of the magnetic flux and the variation becomes very important when the value of n is fixed at the value 2 and for $\tau = 1$. This result is very similar to the previous results obtained in [28, 42]. We conclude that the wedge disclination n is a physical quantity that

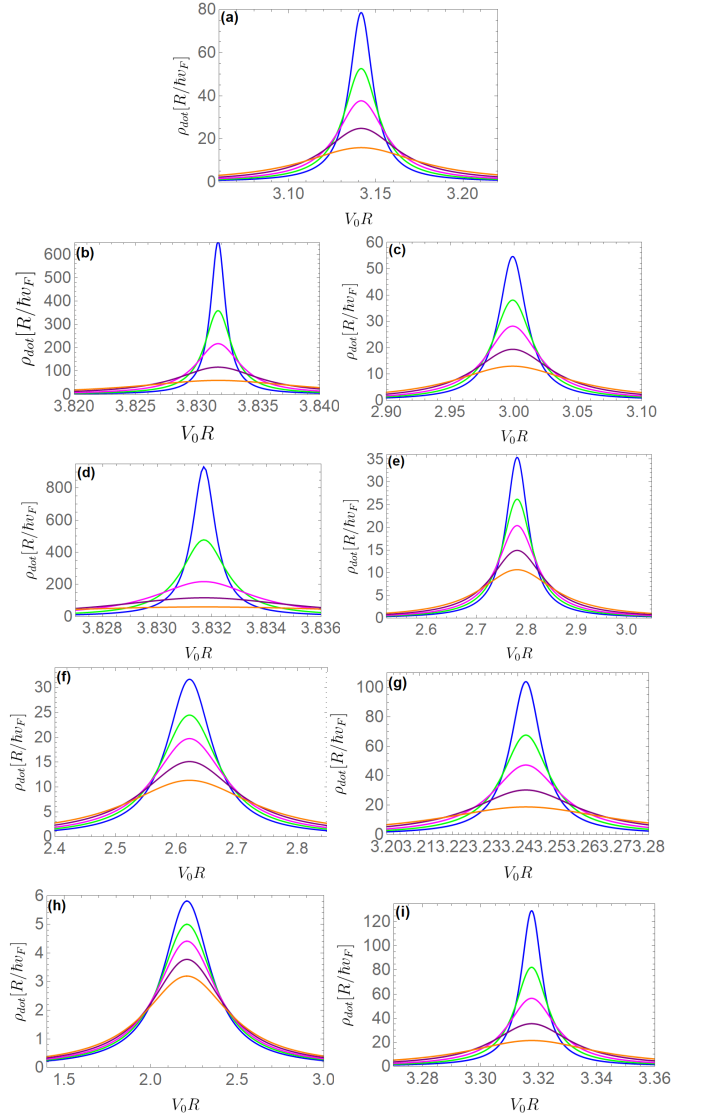


FIG. 9. (color online) DOS as a function of gate voltage $V_0 R$ at $\epsilon = 0$ with $\Phi_i = 1/2$ and for the first resonance $\mu = 1$ by changing the ratio $R/L = 0.08$ (blue line), $R/L = 0.1$ (green line), $R/L = 0.13$ (magenta line), $R/L = 0.16$ (purple line), $R/L = 0.2$ (orange line). With the pair (n, τ) such that (a): 0, (b): $(1, 1)$, (c): $(1, -1)$, (d): $(2, 1)$, (e): $(2, -1)$, (f): $(-1, 1)$, (g): $(-1, -1)$, (h): $(-2, 1)$, (i): $(-2, -1)$.

can alter the behavior of the resonance peaks that make up the DOS. Furthermore, its effect is amplified in the presence of a magnetic flux. As a result, we can say that it can be used as a tunable physical parameter for the control of the transport properties of our system.

VI. CONCLUSION

We considered a model of graphene quantum dot in the presence of magnetic flux Φ_i undergoing a defect, which can be understood from Volterra's constructions.

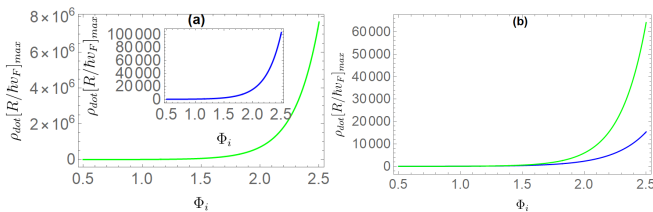


FIG. 10. (color online) Amplitude of the resonance peak as function of the magnetic flux Φ_i at $\epsilon = 0$ with $R/L = 0.2$ for $n = 1$ (blue line), $n = 2$ (green line) and $V'_0 R = V_0 R$.

To treat the problem properly, we started by solving the corresponding Dirac equation and analytically determining the energy spectra, taking into account the cylindrical symmetry. We found that the solutions are expressed in terms of Hankel functions. Then, we obtained an approximate formula for the density of states (DOS) as a function of physical parameters such as magnetic flux, angular momentum, wedge disclination, and applied electrostatic potential.

The analysis of the results shows that even if graphene does not present a gap in its electronic energy spectrum, we can have the confinement of electrons under the effect of an external electrostatic excitation in a quantum dot surrounded by a large sheet of undoped graphene. We have shown that the density of states is an alternative

technique that can be used to study the phenomenon of fermions confinement in a graphene quantum dot. We have performed an analysis that considers the integrated density of states on the dot and an undoped graphene sheet. The formalism we have followed in this paper can easily be extended to this type of measurement configuration. However, with respect to the qualitative analysis of the width, amplitude, and position of the peaks as well as the suppression and creation of new resonance peaks.

We presented our numerical results in terms of the R/L ratio, Φ_i magnetic flux, and wedge disclination n . We have shown that the presence of wedge disclination modifies the behavior of the resonance peaks and also changes their positions. We found that for negative values of n , they can create new resonance peaks and minimize the resonance phenomenon by decreasing the amplitude of the peaks and increasing their widths, thus increasing the number of bound electron states. On the other hand, we have shown that the result of adding a positive n term that represents the defect is a narrow peak that becomes very narrow in the presence of magnetic flux as well as the suppression of some peaks. Finally, we discovered that the density of states is very divergent in the presence of a very strong magnetic field and large values of $n = 2$ (square defect). These results could have potential applications in nanoelectronics.

-
- [1] K. S. Novoselov, A. K. Geim, S. V. Morozov, D.-e. Jiang, Y. Zhang, S. V. Dubonos, I. V. Grigorieva, and A. A. Firsov, Electric field effect in atomically thin carbon films, *science* **306**, 666 (2004).
 - [2] J.-H. Chen, C. Jang, S. Xiao, M. Ishigami, and M. S. Fuhrer, Intrinsic and extrinsic performance limits of graphene devices on SiO_2 , *Nature nanotechnology* **3**, 206 (2008).
 - [3] A. K. Geim and K. S. Novoselov, The rise of graphene, in *Nanoscience and technology: a collection of reviews from nature journals* (World Scientific, 2010) pp. 11–19.
 - [4] F. Schedin, A. K. Geim, S. V. Morozov, E. W. Hill, P. Blake, M. I. Katsnelson, and K. S. Novoselov, Detection of individual gas molecules adsorbed on graphene, *Nature materials* **6**, 652 (2007).
 - [5] A. C. Neto, F. Guinea, N. M. Peres, K. S. Novoselov, and A. K. Geim, The electronic properties of graphene, *Reviews of modern physics* **81**, 109 (2009).
 - [6] J. Martin, N. Akerman, G. Ulbricht, T. Lohmann, J. v. Smet, K. Von Klitzing, and A. Yacoby, Observation of electron-hole puddles in graphene using a scanning single-electron transistor, *Nature physics* **4**, 144 (2008).
 - [7] A. Das, S. Pisana, B. Chakraborty, S. Piscanec, S. K. Saha, U. V. Waghmare, K. S. Novoselov, H. R. Krishnamurthy, A. K. Geim, A. C. Ferrari, *et al.*, Monitoring dopants by raman scattering in an electrochemically top-gated graphene transistor, *Nature nanotechnology* **3**, 210 (2008).
 - [8] K. Novoselov, S. Morozov, T. Mohinddin, L. Ponomarenko, D. Elias, R. Yang, I. Barbolina, P. Blake, T. Booth, D. Jiang, *et al.*, Electronic properties of graphene, *physica status solidi (b)* **244**, 4106 (2007).
 - [9] A. F. Young and P. Kim, Quantum interference and klein tunnelling in graphene heterojunctions, *Nature Physics* **5**, 222 (2009).
 - [10] O. Klein, Die reflexion von elektronen an einem potenzialsprung nach der relativistischen dynamik von dirac, *Zeitschrift für Physik* **53**, 157 (1929).
 - [11] M. Katsnelson, K. Novoselov, and A. Geim, Chiral tunnelling and the klein paradox in graphene, *Nature physics* **2**, 620 (2006).
 - [12] J. M. Pereira Jr, V. Mlinar, F. Peeters, and P. Vasilopoulos, Confined states and direction-dependent transmission in graphene quantum wells, *Physical Review B* **74**, 045424 (2006).
 - [13] A. Matulis and F. M. Peeters, Quasibound states of quantum dots in single and bilayer graphene, *Physical Review B* **77**, 115423 (2008).
 - [14] J. H. Bardarson, M. Titov, and P. Brouwer, Electrostatic confinement of electrons in an integrable graphene quantum dot, *Physical review letters* **102**, 226803 (2009).
 - [15] B. Dóra, M. Gulácsi, and P. Sodano, Majorana zero modes in graphene with trigonal warping, *physica status solidi (RRL)–Rapid Research Letters* **3**, 169 (2009).
 - [16] P. Recher and B. Trauzettel, Quantum dots and spin qubits in graphene, *Nanotechnology* **21**, 302001 (2010).
 - [17] L. A. Ponomarenko, F. Schedin, M. I. Katsnelson, R. Yang, E. W. Hill, K. S. Novoselov, and A. K. Geim,

- Chaotic dirac billiard in graphene quantum dots, *Science* **320**, 356 (2008).
- [18] A. Jacobsen, P. Simonet, K. Ensslin, and T. Ihn, Transport in a three-terminal graphene quantum dot in the multi-level regime, *New Journal of Physics* **14**, 023052 (2012).
 - [19] S. K. Hämäläinen, Z. Sun, M. P. Boneschanscher, A. Upstu, M. Ijäs, A. Harju, D. Vanmaekelbergh, and P. Liljeroth, Quantum-confined electronic states in atomically well-defined graphene nanostructures, *Physical Review Letters* **107**, 236803 (2011).
 - [20] A. De Martino, L. Dell'Anna, and R. Egger, Magnetic confinement of massless dirac fermions in graphene, *Physical review letters* **98**, 066802 (2007).
 - [21] G. Pal, W. Apel, and L. Schweitzer, Electric transport through circular graphene quantum dots: Presence of disorder, *Physical Review B* **84**, 075446 (2011).
 - [22] M. Calvo, Electrostatic quantum dots in a suspended graphene monolayer, *Physical Review B* **84**, 235413 (2011).
 - [23] J. De Souza, C. de Lima Ribeiro, and C. Furtado, Bound states in disclinated graphene with coulomb impurities in the presence of a uniform magnetic field, *Physics Letters A* **378**, 2317 (2014).
 - [24] T. Choudhari and N. Deo, Graphene with wedge disclination in the presence of intrinsic and rashba spin orbit couplings, *EPL (Europhysics Letters)* **108**, 57006 (2014).
 - [25] J. Heinel, M. Schneider, and P. W. Brouwer, Interplay of aharonov-bohm and berry phases in gate-defined graphene quantum dots, *Physical Review B* **87**, 245426 (2013).
 - [26] M. Schneider and P. W. Brouwer, Resonant scattering in graphene with a gate-defined chaotic quantum dot, *Physical Review B* **84**, 115440 (2011).
 - [27] M. Schneider and P. W. Brouwer, Density of states as a probe of electrostatic confinement in graphene, *Physical Review B* **89**, 205437 (2014).
 - [28] A. Bouhlal, A. Jellal, and H. Bahlouli, Density of states analysis of electrostatic confinement in gapped graphene, *Solid State Communications* **333**, 114335 (2021).
 - [29] C. Furtado, B. G. da Cunha, F. Moraes, E. B. de Mello, and V. Bezzerra, Landau levels in the presence of disclinations, *Physics Letters A* **195**, 90 (1994).
 - [30] M. A. Vozmediano, M. Katsnelson, and F. Guinea, Gauge fields in graphene, *Physics Reports* **496**, 109 (2010).
 - [31] F. Guinea, M. Katsnelson, and A. Geim, Energy gaps and a zero-field quantum hall effect in graphene by strain engineering, *Nature Physics* **6**, 30 (2010).
 - [32] P. Ghaemi, J. Cayssol, D. N. Sheng, and A. Vishwanath, Fractional topological phases and broken time-reversal symmetry in strained graphene, *Physical Review Letters* **108**, 266801 (2012).
 - [33] P. E. Lammert and V. H. Crespi, Topological phases in graphitic cones, *Physical review letters* **85**, 5190 (2000).
 - [34] A. Rüegg and C. Lin, Bound states of conical singularities in graphene-based topological insulators, *Physical Review Letters* **110**, 046401 (2013).
 - [35] Y. V. Nazarov, Y. Nazarov, and Y. M. Blanter, *Quantum transport: introduction to nanoscience* (Cambridge university press, 2009).
 - [36] J. Langer and V. Ambegaokar, Friedel sum rule for a system of interacting electrons, *Physical Review* **121**, 1090 (1961).
 - [37] M. Büttiker, Capacitance, admittance, and rectification properties of small conductors, *Journal of Physics: Condensed Matter* **5**, 9361 (1993).
 - [38] M. Büttiker, H. Thomas, and A. Prêtre, Current partition in multiprobe conductors in the presence of slowly oscillating external potentials, *Zeitschrift für Physik B Condensed Matter* **94**, 133 (1994).
 - [39] M. Büttiker, Time-dependent transport in mesoscopic structures, *Journal of Low Temperature Physics* **118**, 519 (2000).
 - [40] F. T. Smith, Lifetime matrix in collision theory, *Physical Review* **118**, 349 (1960).
 - [41] M. Titov, P. Ostrovsky, I. Gornyi, A. Schuessler, and A. Mirlin, Charge transport in graphene with resonant scatterers, *Physical review letters* **104**, 076802 (2010).
 - [42] A. Gutiérrez-Rubio and T. Stauber, Mass-profile quantum dots in graphene and artificial periodic structures, *Physical Review B* **91**, 165415 (2015).